

Electronic structure and stability of different crystal phases of magnesium oxide

M. Causà, R. Dovesi, C. Pisani, and C. Roetti

Institute of Theoretical Chemistry, University of Turin, via P. Giuria 5, I-10125 Torino, Italy

(Received 2 August 1985)

Three different crystal phases of magnesium oxide [$B1$ (NaCl), $B2$ (CsCl), and $B8_1$ (inverse NiAs)] are investigated theoretically. An *ab initio* all-electron linear combination of atomic orbitals Hartree-Fock approximation is adopted; extended basis sets are used which have been variationally optimized in each case. In ordinary conditions, the $B8_1$ and $B2$ structures result less stable with respect to the rocksalt structure by 0.44 and 1.77 eV, respectively. With increasing pressure, the transition $B1 \rightarrow B2$ is estimated to occur around 2.2 Mbar, while it is not excluded that a pressure interval exists around 2 Mbar where the $B8_1$ phase is the most stable of the three structures. Data on the electronic properties of the three phases are provided and discussed: Mulliken populations, charge-density distribution, electron momentum distribution and anisotropy, magnesium core deformation, and band structure.

I. INTRODUCTION

In connection with problems of material science and geophysics, there has been a renewed interest in factors determining the crystal structure of complex solids. For a comprehensive presentation of the different aspects of this subject, reference can be made to the contributions contained in a recent review book.¹ Semiquantitative correlative schemes, based on different properties of the constituent atoms, have been proposed, which are generally successful in predicting the stable crystal structures within a given class of compounds. For relatively simple systems, a direct approach to the problem is now becoming feasible: it consists of calculating and comparing with each other the cohesive energy of different hypothetical structures. For this purpose, *ab initio* computational schemes must be used with a high degree of sophistication, since very small differences have to be revealed between relatively enormous total crystal energies. As a consequence, such an approach entails a substantial computational effort and does not lend itself to providing simple predictive schemes for application to a number of different compounds. In return, it produces valuable information on the electronic structure of the system under investigation, and its use can be extended in a natural way to the study of other problems of crystal physics, such as, for instance, structure and stability of surfaces, defect concentration and mobility, and so on. Remarkable successes have been achieved along this line through the use of a pseudopotential technique, in conjunction with a local-density *ab initio* Hamiltonian.²⁻⁶ Getting rid of core electrons from the start has two main advantages: First, much smaller energy terms have to be handled and compared with each other; second, with "soft-core" pseudopotentials the wave function of valence electrons is relatively smooth and can usually be described very accurately using as a basis set a reasonable number of plane waves, with great simplifications in the computational procedure. An alternative computational scheme⁷⁻⁹ of comparable sophistication and accuracy can be used for the solution of the same

problem. It is based on an *ab initio* all-electron crystalline-orbital LCAO (linear combination of atomic orbitals) HF (Hartree-Fock) approximation. This computational procedure has some drawbacks with respect to the pseudopotential one; in particular, the nonorthogonality of basis functions can give rise to linear-dependence problems; correlation effects have to be evaluated *a posteriori*, while they are included self-consistently (though in an approximate way) in schemes that adopt a local exchange and correlation potential; the presence of core electrons in the calculation makes it impossible, for the time being, to treat systems containing high-atomic-number atoms. The LCAO-HF procedure has, however, some undeniable merits. The exchange term is treated exactly, which is very important when short-range repulsive forces have to be accurately evaluated; the variational character of the computation makes it possible to choose in an unbiased way the best basis set within a given functional space; as a consequence, relatively few atomic orbitals (AO's) per molecular unit can accurately describe the electronic structure; easy reference can be made to current interpretative schemes in molecular quantum chemistry; finally, the all-electron character of the computation allows us to reveal possible deformations of the cores in the crystalline field. Regarding the crystal-structure problem that concerns us here, we believe that the HF total energies can be used with great confidence since correlation contributions do not usually differ appreciably from one hypothetical structure to another.

In the present paper the LCAO-HF procedure is applied to the calculation of the relative stability and the electronic structure of three different crystal phases of magnesium oxide. Knowledge about the polymorphs of one of the major components of the earth's mantle will enable a better understanding of the crystal chemistry in the earth's interior.¹⁰ Figure 1 represents the three structures and the associated geometrical parameters. Phase $B1$ (NaCl) is the stable one in ordinary conditions, and very rich information is available about its properties. The transition from phase $B1$ to phase $B2$ (CsCl) is well

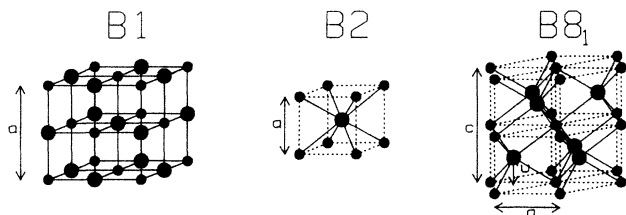


FIG. 1. Crystal structures of magnesium oxide considered in the present work, labeled by their Pearson symbols. Magnesium and oxygen atoms are identified by small and large solid circles, respectively. Phase $B8_1$ is characterized by three parameters, a , c , and u (distance of a layer of oxygen ions parallel to the basal plane from the underlying layer of magnesium ions); in the case of perfect octahedral coordination of the magnesium ions with respect to oxygen, $a/c = \sqrt{3/8}$ and $u/c = 0.25$.

known in halides and has been found to occur in BaO (Ref. 11) and CaO (Ref. 12) at pressures around 150 and 650 kbar, respectively; no such transition has been observed in MgO below 1 Mbar (in the earth's mantle pressures can reach as high as 1.4 Mbar). The possibility of the $B1 \rightarrow B2$ transition has been considered in a number of theoretical investigations, based on widely different approaches. Cohen and Gordon¹³ used a modified electron-gas (MEG) model for evaluating short-range interactions between ions; the O^{2-} ions stabilized by the crystal field were described according to the Watson (+1 well) model¹⁴ or the Yamashita model.¹⁵ The model calculation by Singh and Sanyal¹⁶ employs complicated interionic potentials with parameters fitted against a number of static and dynamical properties of the crystals. The Korringa-Kohn-Rostoker (KKR) investigation of Yamashita and Asano¹⁷ was based on a local-density description of the exchange and correlation potential¹⁸ and on the use of the frozen-core and muffin-tin approximations; the latter is believed to be the main source of error in the determination of total energies by this method. Recently, Chang and Cohen¹⁵ have performed a very accurate study of the $B1$ and $B2$ phases using the pseudopotential *ab initio* approach previously mentioned. As much as 1120 plane waves per molecular unit were used, which is believed to provide an accurate description of valence electrons, and of the static and dynamical properties of the two structures up to pressures above 10 Mbar. That investigation is nearest to the present one in method and scope, and will be often referred to in the following as CC. The pressure for the transition $B1 \rightarrow B2$ calculated in these studies covers a wide range, from 1.17 Mbar (Ref. 16) to 10.5 Mbar (Ref. 5). According to Navrotsky,¹⁹ the former transition is less likely to occur than is the transition from the rocksalt phase to phase $B8_1$ (inverse NiAs), as is observed in a number of sulfides, selenides, tellurides, and transition-metal oxides. By extrapolating a curve based on available data and correlating the standard free energy for the transition $B1 \rightarrow B8_1$ with the standard formation energy of the rocksalt phase, Navrotsky estimates a transition pressure of about 3 Mbar in the case of magnesium oxide. To our knowledge, no *ab initio* theoretical treatment of the NiAs phase of MgO has appeared to date.

The plan of the present work is as follows: In Sec. II

the choice of the basis set for the different structures and lattice parameters is discussed in a rather detailed way; this is, in fact, a very important problem when small energy differences must be revealed. In Sec. III the results are presented and discussed. Energy data are first considered, both concerning the equilibrium conformation and the behavior at high pressures. The electronic structures of the three crystal phases are compared to each other; particular attention is given to electron momentum distributions where anisotropy effects appear more clearly. Finally, the valence-band structures are reported and commented on with reference to the CC results.

II. BASIS-SET PROBLEMS

The variational optimization of the basis set for the various crystal phases in the different geometrical configurations has required the evaluation of more than one-hundred energy points. In order to reduce costs, the computational parameters that control the truncation of the Coulomb and exchange series have been fixed to values for which the residual numerical error is not entirely negligible. The most unfavorable situation occurs with the $B8_1$ phase, which has twice as many atoms in the unit cell and half the number of symmetry operators with respect to the other two structures. In that case the numerical error associated with the truncation parameters that were adopted was estimated to be around 0.1 eV per molecular unit; in the two other cases it was considerably smaller. As will appear in the following, such a numerical error is not a constant since the effectiveness of the truncation criteria in a direct-space approach depends in a complicated way on basis set, crystal geometry, and lattice parameters. The computational cost was not the only problem to be faced; with very large basis sets or with crystal configurations and atomic-orbital sizes giving rise to large overlaps, pseudo-linear-dependence between basis functions may appear, giving rise to catastrophic behavior. Within the limits imposed by these problems, the strategy adopted for the basis-set optimization is discussed in the following; reference is made to the set reported in Table I, which has been used for all the calculations concerning the $B1$ phase at the conformational minimum.

For oxygen we started from the basis set used in the previous study of lithium oxide.²⁰ It is essentially a split-valence set (3 *s*- and 6 *p*-type functions) derived from a standard 6-GTO (Gaussian-type orbitals) basis set.²¹ The exponent α of the single Gaussian in the $3sp$ shell has been optimized for the different conditions. As expected, the results for phases $B1$ and $B8_1$ are very similar, while phase $B2$ requires the use of a larger outer Gaussian (at equilibrium, the optimum α exponent is 0.18 a.u. for $B2$, to be compared with $\alpha = 0.21$ a.u. in the two other cases). When compressing or expanding the crystal, the optimum exponent is also changed, but to a much lesser extent than that corresponding to a geometrical scale factor: for $B1$, $\alpha = 0.20$ and 0.22 a.u. for lattice-parameter values of $a = 4.45$ and 3.90 Å, respectively. Only for the $B1$ phase at equilibrium did we explore the effect of releasing the outer Gaussian ($\alpha = 0.53642$ a.u.) of the oxygen $2sp$ shell,

TABLE I. Exponents (in a.u.) and coefficients of the Gaussian functions used for the calculation of the $B1$ phase at the conformational minimum. The contraction coefficients multiply normalized individual Gaussians. In other calculations the Gaussians labeled by an asterisk may have been used in a different way, by changing the exponent, or by using them as independent functions, or by dropping them altogether (see text and Table II).

Atom	Shell	Type	Gaussian	Exponent	Coefficient	
					s	p
Magnesium	1	s	1	68 371.9	0.000 222 6	
			2	9 699.34	0.001 898 2	
			3	2 041.18	0.011 045 1	
			4	529.863	0.050 062 7	
			5	159.186	0.169 123	
			6	54.684 8	0.367 031	
			7	21.235 7	0.400 410	
			8	8.746 04	0.149 870	
	2	sp	9	156.795	-0.006 24	0.007 72
			10	31.033 9	-0.078 82	0.064 27
			11	9.645 3	-0.079 92	0.210 4
			12	3.710 9	0.290 63	0.343 14
			13*	1.611 64	0.571 64	0.373 50
			14*	0.642 944	0.306 64	0.232 86
	3	sp	15*	0.4	1.0	1.0
Oxygen	1	s	1	4 000.	0.001 44	
			2	1 355.58	0.007 64	
			3	248.545	0.053 7	
			4	69.533 9	0.168 18	
			5	23.886 8	0.360 39	
			6	9.275 93	0.386 12	
			7	3.820 34	0.147 12	
			8	1.235 14	0.071 05	
	2	sp	9	52.187 8	-0.008 73	0.009 22
			10	10.329 3	-0.089 79	0.070 68
			11	3.210 34	-0.040 79	0.204 33
			12	1.235 14	0.376 66	0.349 58
			13*	0.536 42	0.422 48	0.277 74
	3	sp	14*	0.21	1.0	1.0

TABLE II. Influence of the basis set of magnesium on total energy, kinetic energy, and magnesium Mulliken net charge for the $B1$ phase of MgO at the experimental lattice parameter. ΔE_j (ΔT_j) is the total- (kinetic-) energy difference between case j and case 1 ($E_1 = -274.6601$ $T_1 = 274.7214$ a.u.). The oxygen basis set reported in Table I has been used for all cases; the reference "ionic" Mg basis includes the first two shells of Table I, and corresponds to an optimized isolated Mg^{2+} solution; the other six bases have been obtained from the reference one by releasing the outer Gaussian of the $2sp$ shell (G14 in case 2, G13 and G14 in case 3) or by adding an additional s (case 4) or sp (cases 5–7) shell with exponent α . Case 6 corresponds to Table I.

Case	Mg basis	Number of Mg AO's	ΔE (a.u.)	ΔT (a.u.)	Mg net charge
1	ionic	5			+ 2.00
2	split G14	9	-0.0025	-0.10	+ 2.01
3	split G13,G14	13	-0.0028	-0.13	+ 2.01
4	+ s ($\alpha=0.4$)	6	-0.0006	-0.01	+ 2.00
5	+ sp ($\alpha=0.35$)	9	-0.0029	-0.03	+ 1.96
6	+ sp ($\alpha=0.40$)	9	-0.0024	-0.04	+ 1.98
7	+ sp ($\alpha=0.45$)	9	-0.0021	-0.05	+ 1.99

TABLE III. Magnesium-ion relaxation energy (ΔE^{rel}) as a function of the lattice parameter (a) for the $B1$ phase. ΔE^{rel} is defined as the difference between the total energies obtained using an ionic contracted or uncontracted basis set (cases 1 and 2 Table II, respectively). The corresponding change in kinetic energy (ΔT^{rel}) is also reported. The last row refers to the isolated ion.

a (Å)	ΔE^{rel} (a.u.)	ΔT^{rel} (a.u.)
3.70	0.0095	0.49
3.80	0.0056	0.34
3.90	0.0030	0.27
4.20	0.0025	0.10
4.45	0.0023	0.07
∞	0.0001	0.05

i.e., using it as an independent function. The energy gain associated with this additional variational freedom was very small, of the same order as for the isolated atom, but could become more important in compressed structures.

For magnesium two points were considered, the need for valence $3sp$ functions and the relaxation of the ion in the crystal field. The $1s$ and $2sp$ functions reported in Table I correspond to a very accurate solution for the isolated Mg^{2+} ion, and form what we call the ionic set. The effect of enriching the ionic set is documented in Table II, with reference to the $B1$ phase at equilibrium: Split-core sets (cases 2 and 3) serve to explore the importance of ion relaxation, while the addition of an outer "valence" shell

(cases 4–7) permits, in principle, less ionic configurations to be realized. It is seen that the population of the additional valence shell increases regularly with increasing orbital size, but always remains very small, thus confirming the fully ionic character of magnesium oxide. The energy gain associated with the additional variational freedom is, in all cases, less than 0.1 eV, and split-core sets perform about equally well as core-plus-valence sets. In compressed crystals, core-relaxation effects become more important, as shown in Table III; frozen-core approximations could become questionable at very high pressures. Split-core sets corresponding to case 2 of Table II have been used for the $B1$ and $B8_1$ phases when considering V/V_0 values below 0.85, and in all cases for the $B2$ structure.

III. RESULTS AND DISCUSSION

The dependence of energy on the geometrical parameters was investigated using the criteria discussed in the preceding section. The results are reported in Table IV. Note that in all cases the kinetic energy is quite close to the absolute value of the total HF energy, which is good check of the accuracy of the calculation. For the calculation of the HF cohesive energy, we have subtracted the minimum total energy E per molecular unit in the crystal from the sum of the HF energies of the isolated atoms. The latter were obtained using the best basis set within the same functional space that was variationally explored for describing the crystals (see Sec. II): their values

TABLE IV. Energy data and geometrical parameters at equilibrium, and parameters for Murnaghan's equation of state for the three crystal structures.

	Crystal structure			
	Calc.	$B1$ Expt.	$B2$ Calc.	$B8_1$ Calc.
Energy data at equilibrium (a.u. per molecule)				
HF total energy E_0^{HF}	-274.663		-274.598	-274.647
HF kinetic energy T_0^{HF}	274.642		274.651	274.665
HF cohesive energy E_c^{HF}	0.267		0.202	0.251
Total cohesive energy E_c	0.366	0.384 ^a	0.301	0.350
Geometrical equilibrium parameters (Å)				
a_0	4.201	4.21	2.573	2.900
c_0				4.988
Parameters of Murnaghan equation of state (a.u.)				
V_0	125.10	125.90	115.07	122.60
B	0.00631	$\left\{ \begin{array}{l} 0.00551^{\text{b}} \\ 0.00527^{\text{c}} \\ 0.00605^{\text{d}} \end{array} \right.$	0.00656	0.00631
B'	3.53		2.94	3.47

^aSee Ref. 24.

^bSee Ref. 26.

^cSee Ref. 27.

^dSee Ref. 28.

are $E_{\text{Mg}} = -199.6037$ a.u. and $E_{\text{O}} = -74.7928$ a.u., to be compared with the respective HF limits $E_{\text{Mg}}^{\text{HF}} = -199.6146$ a.u. and $E_{\text{O}}^{\text{HF}} = -74.8094$ a.u. The contribution of correlation effects to the cohesive energy was evaluated by considering the nearly perfect ionic character of the crystals (see below); that is, summing—in all cases—the difference in correlation energy between O^{2-} and O (-0.148 a.u.) (Ref. 22) to the difference in correlation energy between Mg and Mg^{2+} (0.049 a.u.) (Ref. 23). The experimental cohesion energy for the rock-salt phase at zero temperature, as obtained from thermodynamic data,²⁴ is reasonably close to the calculated result. The corresponding equilibrium lattice parameter is also very near the observed value. Phase *B2* appears to be unstable with respect to phase *B1* at zero pressure by 0.065 a.u., which is similar to the result of CC (0.055 a.u.); the other theoretical determinations are scattered over a relatively wide range: 0.027 ,¹⁷ 0.124 , 0.150 ,¹³ and 0.209 a.u.¹⁶ On the other hand, the equilibrium lattice parameter for phase *B2* (2.574 Å) is appreciably smaller with respect to the CC determination (2.628 Å) and is closer to that reported by Yamashita and Asano,¹⁷ 2.593 Å. The determination of the equilibrium structure for phase *B8₁* involves, in principle, three parameters, a , c , and u (see Fig. 1). However, reducing the crystal symmetry by displacing the layers of oxygen atoms parallel to the basal plane with respect to their central position between adjacent magnesium layers (i.e., changing the u value from $c/4$) results in a net energy increase. The optimization of the other two parameters results in a slight stretching in the c direction (the c/a ratio is changed from 1.633 , as in the ideal octahedral case, to 1.72), but the molecular volume is approximately the same as in the rock-salt phase, and the gain in energy associated with that stretching is minute (less than 0.1 eV). It can be noticed that the NiAs phase is nearly as stable as the NaCl one, which is expected because of the similarity of the two structures. Table IV also reports the parameters of the Murnaghan equation of state²⁵ for the three structures:

$$E(V) = E_0 + (BV/B')[(V_0/V)^{B'} / (B' - 1) + 1] - V_0 B / (B' - 1).$$

A few comments can be made upon these data: (a) The parameters have been obtained by fitting HF energies; it is therefore implicitly assumed that correlation energy is not appreciably dependent on volume and crystal structure. On the other hand, changes in correlation energy over the explored range are probably less important than the uncertainty associated with basis-set effects. (b) For the hexagonal *B8₁* phase, due to the high cost of the computations, only isotropic compression was considered, with conservation of the ideal octahedral structure. We do not believe that taking into account crystal deformation would matter very much since the energy gains associated with the optimization of the c/a ratio were only slightly beyond the present numerical precision. (c) The range of V values explored was relatively small; the problems of pseudo-linear-dependence mentioned in Sec. II prevented us from considering V/V_0 ratios below about 0.7 .

Figure 2 shows the best-fit $E(V)$ curves and the energy data on which they are based, in order to give a more pre-

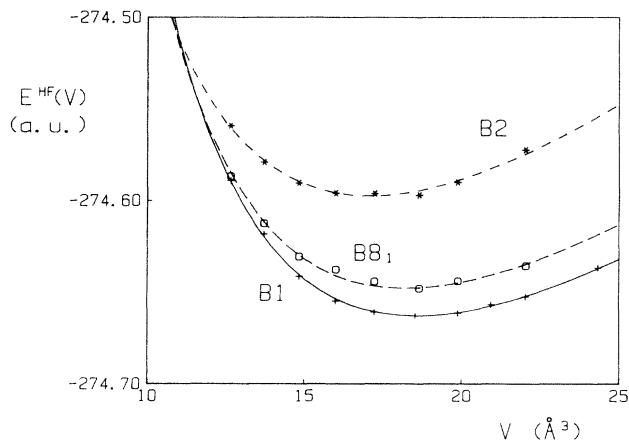


FIG. 2. Hartree-Fock energies for the three crystal structures as a function of molecular volume. The symbols indicate calculated points; the curves correspond to the Murnaghan equation with the best-fit parameters listed in Table IV.

cise idea of the number and range of data points, and of their dispersion about the best-fit curve; it is apparent that the quality of the *B8₁* results is poorer than for the other two structures for the reasons mentioned in the preceding section. The numerical error affecting the parameters within the present model was roughly estimated by considering, for each crystal structure, the results obtained with different subsets of data points. As expected, B' is the parameter affected by the largest relative error, while E_0 and V_0 are very accurately determined. The error in the B parameter (bulk modulus) was estimated to be about 2% for the rock-salt phase. The present estimate of the bulk modulus (1.86 Mbar) is somewhat too high with respect to the experimental determinations, 1.62 Mbar, obtained by ultrasonic interferometry,²⁶ 1.55 Mbar, obtained from neutron-scattering data,²⁷ and 1.78 Mbar, resulting from compression measurements;²⁸ it is still more at variance with the CC determination, 1.46 Mbar, but close to the KKR result,¹⁷ 1.71 Mbar. Inclusion of zero-point motion effects, acting as a negative pressure, could improve the agreement with the experimental data.⁴

Figure 3 illustrates the dependence on pressure of the zero-temperature free energy ($G = E + pV$) of the *B2* and *B8₁* phases, referred to $G_{B_1}(p)$, the free energy of the rock-salt phase. It is seen that G_{B_2} becomes less than G_{B_1} around 2.2 Mbar; this is still too high for the transition to occur in the earth's interior. Note, however, that the present estimate is much lower than that by CC (10.5 Mbar); this difference is far beyond possible extrapolation errors. The molecular volumes at 2.2 Mbar are 11.65 and 10.39 Å³ for the *B1* and *B2* phases, respectively; the transition-volume change, $\Delta V_t = 1.26$ Å³, is appreciably larger than that predicted by CC (0.33 Å³). Since the difference between the molecular volumes does not depend very much on pressure, and due to the term pV in the free-energy expression, we can expect, in general, that high calculated transition pressures Δp_t correspond to small volume differences at zero pressure, ΔV_0 , and vice versa. As a matter of fact, the various calculated values of p_t and ΔV_0 are strictly anticorrelated, as appears from the following list (p_t in Mbar, ΔV_0 in Å³): 1.17 and 4.04

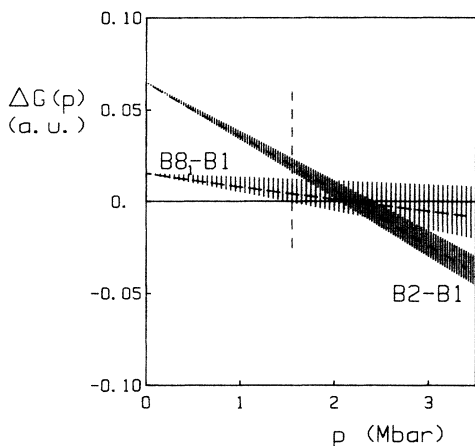


FIG. 3. Difference of the zero-temperature free energy of the $B8_1$ or $B2$ phase with respect to the $B1$ phase ($\Delta G = \Delta E + p \Delta V$), as a function of pressure. The shaded area indicates the estimated margin of error. The calculated points are all located to the left of the vertical dashed line; extrapolation was effected according to the Murnaghan equation, using the parameters listed in Table IV.

(Ref. 16); 2.2 and 1.49 (present calculation); 2.56 and 2.00 (Ref. 13, Watson model for O^{2-}); 3.72 and 1.21 (Ref. 13, Yamashita model for O^{2-}); 10.5 and 0.35 (Ref. 5). The difference between the present description of the relative stability of the two phases and the pseudopotential results can therefore be traced back to the different determinations of the equilibrium configuration of the $B2$ phase. For that crystal structure, characterized by very dense packing of positive and negative ions, the pseudopotential frozen-core approximation might undergo a partial failure. The stability of the NiAs phase at high pressure with respect to the NaCl one is less easily discussed precisely because of the similarity of the two molecular volumes. As shown in Fig. 3, the two free-energy curves run, in fact, nearly parallel to each other, and the intersection point is located approximately at the same pressure as in the preceding case. Due to the relatively high estimated error affecting the results for the $B8_1$ phase, the present investigation does not rule out the possibility that a pressure interval exists, where the NiAs phase is the most stable of the three structures.

Let us now consider the electronic structure of the three crystal phases. In a related paper²⁹ the electron charge and electron momentum distribution of the rocksalt phase of magnesium oxide at the equilibrium configuration have been analyzed accurately, with reference to the rich experimental and theoretical information that is available. The main results of that study were as follows. The classic description of magnesium oxide according to the configuration $Mg^{2+}O^{2-}$ was confirmed to be essentially adequate. The Mulliken gross population on magnesium exceeds ten electrons by less than 0.03 electrons, while bond populations between neighboring ions are very small and slightly negative. Differential charge-density maps with respect to an atomic superposition model clearly exhibit the large charge transfer from the magnesium atom to the valence region of oxygen. On the other hand, the differential charge density is near zero outside core re-

gions when ionic superposition models are taken as a reference, using the classic descriptions of the oxygen ion as stabilized by the crystal field;^{14,15} appreciable differential densities are found in these cases only in the region of the oxygen core, where the present description is intermediate between those obtained using the Watson¹⁴ or Yamashita¹⁵ model, and in the region of the magnesium core, due to a small expansion of that ion in the crystal field. The calculated structure factors are in agreement with experimental determinations^{30,31} within the declared experimental error; the latter is, however, too large for definite statements to be made about the accuracy of the calculated charge density. The electron momentum distribution exhibits appreciable anisotropy (up to about 8% at 1.5 a.u.), which is attributable to orthogonality effects between neighboring oxygen ions. The analysis of the average Compton profiles further supports the ionic model. The present discussion makes reference to those results, and its primary purpose is to evidence the role of crystal structure and pressure on the electronic properties.

Consider first the results of the Mulliken-population analysis. The ionicity is practically complete in all cases, the magnesium population never exceeding 10.05 electrons. It is difficult to identify different degrees of ionization for the three structures because there are changes in Mulliken populations related to modifications of the basis set (see Sec. II) which are of the order of a few hundredths of an electron. The bond population between neighboring ions is always negative; for first-neighbor magnesium and oxygen it is about -0.01 and is negligible for neighboring magnesium ions, in all cases; regarding first-neighbor oxygen ions, the bond population is again -0.01 for the rocksalt and NiAs structures, while it is as large -0.1 for the CsCl structure, where the O-O distance is much smaller. With increasing pressure there are no substantial changes in the above picture; the most important effect is the large increase in the antibonding population between neighboring oxygen ions in the $B2$ phase, which is nearly doubled at $V/V_0 = 0.7$. It is interesting, finally, to briefly comment on the value of the multipoles of the charge distributions assigned to each ion according to the Mulliken analysis. Only in the hexagonal NiAs phase can nonzero multipoles lower than the hexadecapole ones exist by symmetry; in that case the quadrupole moment of the oxygen ion, associated with a slightly different population of the p_z with respect to the p_x and p_y orbitals, is exceedingly small and, in fact, not meaningful. The hexadecapoles of the oxygen ion in the $B1$ and $B8_1$ phases are small in comparison with other anions, such as H^- in LiH (Ref. 9) or N^{3-} in Li_3N (Ref. 33); their sign indicates a compression of the ion in the direction of the neighboring magnesium ions. In the $B2$ phase the hexadecapoles are larger and correspond to ion compression in the direction of the neighboring oxygen ions.

Charge-density data confirm the results of the Mulliken analysis. The charge densities for the three phases at zero pressure are very similar to each other except in the ionic interstices. The conclusions drawn for the $B1$ phase (fully ionic character, slight expansion of the magnesium ion, intermediate character of the oxygen ion between the Watson and Yamashita models) can therefore be extended

TABLE V. Minimum electron charge density along the atom-atom directions for the three phases; $B1$, $B2$, and $B8_1$ refer to the calculated equilibrium structural parameters reported in Table IV. $B1^+$ refers to a calculation performed with $a = 3.70 \text{ \AA}$; numbers in parentheses indicate the distance of the minimum from Mg, in units of $d_{\text{Mg-O}}$. Charge density is expressed of $10^{-4} e^-/\text{a.u.}^3$.

	Crystal structure			
	$B1$	$B1^+$	$B2$	$B8_1$
Mg-Mg	167	308	87	119
O-O	167	308	331	155
Mg-O	347(0.427)	661(0.441)	262(0.418)	355(0.427)

to the other structures. Table V reports some density data at points of interest; the similarity of $B1$ and $B8_1$ phases is again apparent. As noted by CC, compressing the crystal makes the density more uniform; the location of the minimum between nearest-neighbor oxygen and magnesium is progressively displaced toward the middle point of the segment. Although the general features of the present results are similar to those reported by CC, we did not find, in the differential charge densities (calculated minus atomic superposition density), any kind of fine structure such as that appearing in their Fig. 3: those oscillations could be an artifact, associated with their use of the plane-wave basis set.

The electron momentum distribution (EMD), particularly its anisotropy, may reveal interesting features of the electronic structure. Figure 4 describes the EMD anisotropy for the three crystal phases by reporting the differ-

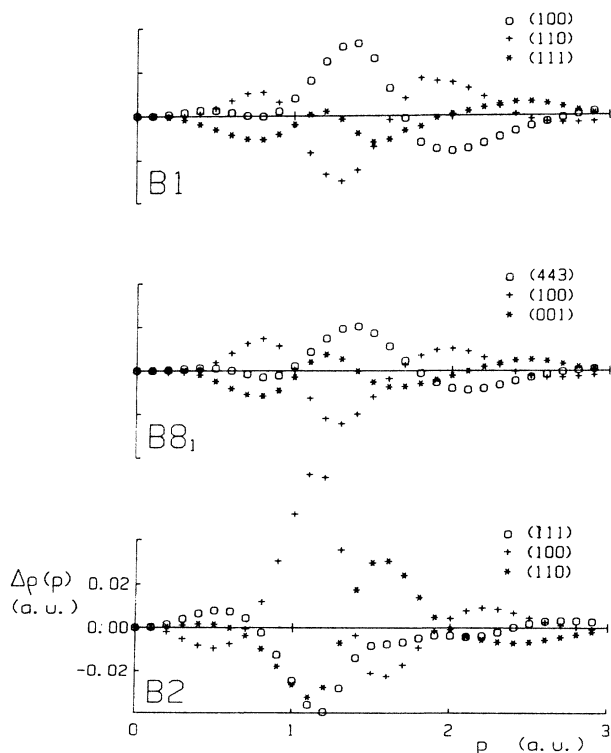


FIG. 4. EMD anisotropies $\Delta\rho_{hkl}(p) = \rho_{hkl}(p) - \bar{\rho}(p)$ as a function of electron momentum p , for the three crystal phases at zero pressure. The same label in the various plots identifies corresponding directions (see text). The scales are the same in all cases and are reported only in the bottom plot.

ence $\Delta\rho(p)$ between the density of electron momenta along assigned crystallographic directions, and the average EMD, $\bar{\rho}(p)$. In the present case the EMD anisotropy has to be entirely attributed to p electrons of oxygen. The selected directions have therefore been chosen to correspond to directions of interest of electron momenta as viewed from a nucleus of oxygen: The first one (identified by open circles) points toward one of the nearest magnesium ions, the second (pluses) toward one of the nearest oxygen atoms, and the third (asterisks) points the farthest from neighboring magnesium ions. The $B1$ and $B8_1$ anisotropies look strikingly similar to each other: In both cases electrons are slowest in the direction of neighboring magnesium ions, and faster in the other two directions, where antibonding oxygen-oxygen interactions are more important. The EMD of the $B2$ structure is much more anisotropic; the oxygen-oxygen direction is clearly distinguished from the others, especially for the large peak of relatively slow electrons about 1 a.u.; high-momentum electrons are also particularly abundant in that direction. Compressing the crystals obviously causes a general increase of electron velocities, which is, however, not uniformly distributed in all directions. This is exemplified in Fig. 5, where the EMD's of the $B1$ phase at $V/V_0 = 1$ and $V/V_0 = 0.68$ are compared to each other. It is seen that there is an important increase of the density of high-momentum electrons moving along the oxygen-oxygen (110) line; the depopulation of slow electrons is quite uniform, while at intermediate momenta (1–2 a.u.) the changes in momentum density along the various directions act in the sense of diminishing the EMD anisotropy with respect to the uncompressed crystal.

A more detailed discussion of the EMD of the oxide ion in different crystal environments is deferred to further work. The analysis will be performed in direct space, by considering the Fourier transform of $\rho(\mathbf{p})$, the so-called autocorrelation function $B(\mathbf{r})$;^{34,35} that representation allows a transparent interpretation of all the important features of the EMD in relation to the crystal structure and chemical properties of the system,³⁶ and permits a direct comparison with experimental data.

Let us finally briefly comment on band structures. The basis sets adopted here, chosen according to strictly variational criteria, do not permit any useful information to be gathered about virtual levels; therefore, the discussion is confined here to valence bands. The oxygen p bands for the $B1$ and $B2$ phases, represented in Fig. 6, are very similar to those reported by CC. The $B8_1$ band structure bears some resemblance to the $B1$ one: along the three-

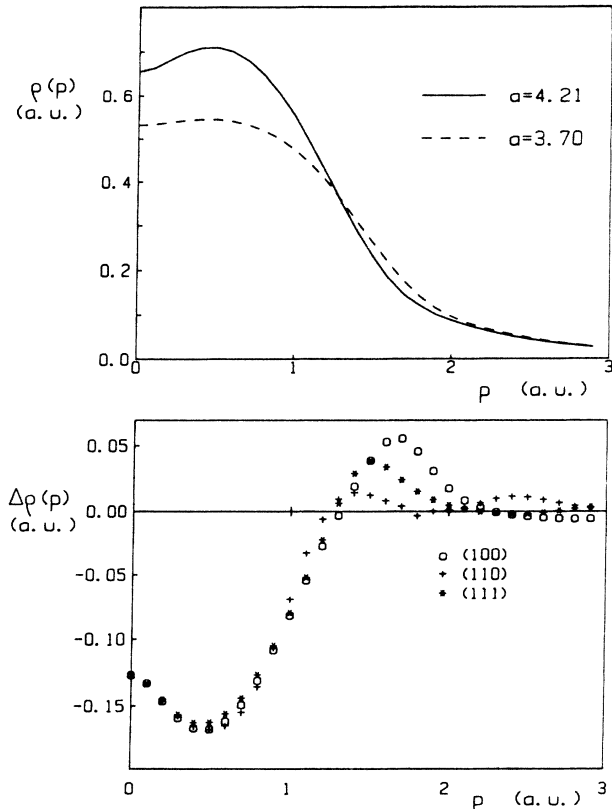


FIG. 5. Effect of compression on EMD and EMD anisotropies. The two cases here considered refer to the $B1$ phase at $V/V_0=1$ ($a=4.21$ Å) and $V/V_0=0.679$ ($a=3.70$ Å). The top plot reports the average momentum density $\bar{p}(p)$ in the two cases. The bottom plot reports the change of momentum density along the three main crystallographic directions, $\Delta p(p) = \rho^{(3.70)}(p) - \rho^{(4.21)}(p)$.

fold symmetry axis (line $L\Gamma$ in $B1$, $A\Gamma$ in $B8_1$), the bands of the hexagonal phase closely correspond to those of the cubic structure folded on themselves, except for the splitting of the threefold-degenerate Γ_{15} level. However, the band minimum for the $B8_1$ phase occurs at H , outside that line: Correspondingly, the bandwidth is appreciably larger than in the $B1$ case. Valence-band widths (see Table VI) are larger than those obtained with the pseudo-

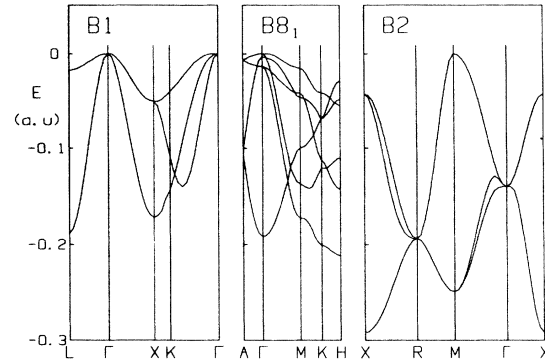


FIG. 6. p -valence band structures for the three phases at equilibrium.

potential technique, but are compatible with experimental data.³⁷

This may be surprising at first sight since the HF approximation is known to exaggerate the spacing of levels; however, this effect is particularly important only in the vicinity of the Fermi level. The effect of compression is a general increase in bandwidths, which is of the same order as obtained with the pseudopotential calculation.

IV. CONCLUSIONS

The results of the present investigation are partially at variance with those of the CC study. The most marked disagreement concerns the estimated transition pressure from the $B1$ to the $B2$ phase, which is much lower in the present case, and the corresponding volume change which is, on the contrary, much larger; the former effect is probably a consequence of the latter. The reason for these discrepancies is not completely clear; the largest errors that affect our calculated energies are due to neglect of correlation and to basis-set effects, which may have a different importance in different conditions, but cannot justify the large difference with respect to the CC results.

For the first time, an *ab initio* study of the NiAs ($B8_1$) structure of magnesium oxide has been performed. According to the present calculations, there is a pressure around 2.2 Mbar where the three phases have about the

TABLE VI. Valence-band widths (total, p and s) for the three crystal phases, at normal and reduced volume. The value 0.754 of the ratio V/V_0 has been chosen in order to allow comparison with CC results. The experimental data are from Ref. 37. Units are eV.

Crystal structure:		$B1$		$B2$		$B8_1$	
V/V_0 :		1	0.754	1	0.754	1	0.754
$\Delta E_v(sp)$	Present	22.9	24.9	22.8	25.0	25.9	27.4
	CC	17.1	19.0			18.3	20.6
	Expt.	21.0					
$\Delta E_v(p)$	Present	5.1	7.0	5.8	9.4	7.9	9.4
	CC	4.8	6.3			6.6	8.5
	Expt.	~5-6					
$\Delta E_v(s)$	Present	1.9	3.1	1.8	3.1	4.1	6.7
	CC	1.7	2.7			3.0	5.0

same free energy. At much higher and lower pressures the $B2$ and $B1$ phases, respectively, are undoubtedly the most stable structures. Due to the uncertainties of the present calculation, it is not excluded that a pressure interval exists where the $B8_1$ structure is the most stable one; the range could include pressures that exist in the earth's interior. If this were the case, it would be worthwhile to perform a more accurate study of the

structural and dynamical properties of phase $B8_1$ in those extreme conditions.

ACKNOWLEDGMENTS

Financial support by the Italian Ministero della Pubblica Istruzione and by the Italian Consiglio Nazionale delle Ricerche is gratefully acknowledged.

-
- ¹*Structure and Bonding in Crystals*, edited by M. O'Keeffe and A. Navrotsky (Academic, New York, 1981), Vols. I and II.
- ²J. Ihm, A. Zunger, and M. L. Cohen, *J. Phys. C* **12**, 4409 (1979).
- ³M. L. Cohen, in *Structure and Bonding in Crystals*, Ref. 1, Vol. I, p. 25.
- ⁴S. Froyen and M. L. Cohen, *Phys. Rev. B* **29**, 3770 (1984).
- ⁵K. J. Chang and M. L. Cohen, *Phys. Rev. B* **30**, 4774 (1984).
- ⁶K. J. Chang and M. L. Cohen, *Phys. Rev. B* **31**, 7819 (1985).
- ⁷C. Pisani and R. Dovesi, *Int. J. Quantum Chem.* **17**, 501 (1980).
- ⁸R. Dovesi, C. Pisani, C. Roetti, and V. R. Saunders, *Phys. Rev. B* **28**, 5781 (1983).
- ⁹R. Dovesi, C. Ermondi, E. Ferrero, C. Pisani, and C. Roetti, *Phys. Rev. B* **29**, 3591 (1984).
- ¹⁰J. C. Jamieson, M. H. Manghnani, and L. C. Ming, in *Structure and Bonding in Crystals*, Ref. 1, Vol. II, p. 95.
- ¹¹L. G. Liu, *J. Appl. Phys.* **42**, 3702 (1971).
- ¹²R. Jeanloz and T. Ahrens, *Science* **206**, 829 (1979).
- ¹³A. J. Cohen and R. G. Gordon, *Phys. Rev. B* **14**, 4593 (1976).
- ¹⁴R. Watson, *Phys. Rev.* **111**, 1108 (1958).
- ¹⁵J. Yamashita and S. Asano, *J. Phys. Soc. Jpn.* **28**, 1143 (1970).
- ¹⁶R. K. Singh and S. D. Sanyal, *Phys. Status Solidi B* **113**, k23 (1982).
- ¹⁷J. Yamashita and S. Asano, *J. Phys. Soc. Jpn.* **52**, 3506 (1983).
- ¹⁸O. Gunnarsson and B. I. Lundqvist, *Phys. Rev. B* **13**, 4274 (1976).
- ¹⁹A. Navrotsky, in *Structure and Bonding in Crystals*, Ref. 1, Vol. II, p. 71.
- ²⁰R. Dovesi, *Solid State Commun.* **54**, 183 (1985).
- ²¹W. J. Hehre, R. F. Stewart, and J. A. Pople, *J. Chem. Phys.* **51**, 2657 (1969).
- ²²E. Clementi, *J. Chem. Phys.* **38**, 2248 (1963).
- ²³E. Clementi, *IBM J. Res. Dev.* **9**, 2 (1965).
- ²⁴E. S. Gaffney and T. J. Ahrens, *J. Chem. Phys.* **51**, 1088 (1969).
- ²⁵F. D. Murnaghan, *Proc. Nat. Acad. Sci. U.S.A.* **30**, 244 (1944).
- ²⁶O. L. Anderson and P. Andreatch, Jr., *J. Am. Ceram. Soc.* **49**, 404 (1966).
- ²⁷M. J. L. Sangster, G. Peckham, and D. H. Saunders, *J. Phys. C* **3**, 1026 (1970).
- ²⁸H. G. Drickamer, R. W. Lynch, R. L. Clendenen, and E. A. Perez-Albuerne, in *Solid State Physics*, edited by F. Seitz and D. Turnbull (Academic, New York, 1966), Vol. 17, p. 135.
- ²⁹M. Causà, R. Dovesi, C. Pisani, and C. Roetti, *Acta Crystallogr. Sect. A* (to be published).
- ³⁰P. L. Sanger, *Acta Crystallogr. Sect. A* **25**, 694 (1969).
- ³¹J. L. Lawrence, *Acta Crystallogr. Sect. A* **29**, 94 (1973).
- ³²K. F. Berggren, S. Manninen, T. Paakkari, O. Aikala, and K. S. Mansikka, in *Compton Scattering*, edited by B. Williams (McGraw-Hill, New York, 1977), p. 139.
- ³³R. Dovesi, C. Pisani, F. Ricca, C. Roetti, and V. R. Saunders, *Phys. Rev. B* **30**, 972 (1984).
- ³⁴W. Schülke, *Phys. Status Solidi B* **82**, 229 (1977).
- ³⁵P. Pattison and W. Weyrich, *J. Phys. Chem. Solids* **40**, 213 (1979).
- ³⁶M. Causà, R. Dovesi, C. Pisani, and C. Roetti, *Phys. Rev. B* **32**, 1196 (1985).
- ³⁷L. Fiermans, R. Hoogewijs, G. de Meyer, and J. Vennik, *Phys. Status Solidi A* **59**, 569 (1980).